Chiral non-stoichiometric silver indium sulfide ternary quantum dots: investigation on the chirality transfer by cysteine

Electronic Supporting Information

Lorenzo Branzi,[1] Finn Purcell-Milton,[2] Chiara Cressoni,[3] Michele Back,[1] Elti Cattaruzza,[1] Adolfo Speghini,[3*] Yurii K. Gun'ko,[2*] Alvise Benedetti[1*]

[1] Department of Molecular Science and Nanosystems, Ca' Foscari University of Venice, Via Torino 155 Venezia Mestre.

[2] School of Chemistry, CRANN and AMBER Research Centres, Trinity College Dublin, College Green, Dublin 2, Ireland.

[3] Nanomaterials Research Group, Department of Biotechnology and INSTM, RU of Verona, University of Verona, Strada le Grazie 15, 37134 - Verona, Italy.

LIST OF CONTENTS

Fig. S1 Particle size distribution Pag. S1

Fig. S2 Phase contrast TEM images of non-stoichiometric AIS QDs Pag. S1

Comment on XPS Analysis Pag. S2

Fig. S3 XPS spectra Pag. S2

Photoluminescence Quantum yield Determination Pag. S3

Photoluminescence Lifetime analysis Pag. S4

Fig. S4 PL decay curve of **L-AIS** QDs solution Pag. S4

Table S1 Parameters of the PL lifetime analysis Pag. S4

Fig. S5 UV/Vis and CD spectra of **L** and **D-AIS** QDs Pag. S5

Fig. S6 plot of the anisotropic g-factor of **L** and **D-AIS** QDs Pag. S5

Investigation on the second reaction step: photoluminescence and structure Pag. S6

Fig. S7 picture of **L-AIS** QDs colloidal solution Pag. S6

Fig. S8 UV/Vis and CS spectra Pag. S7

Fig. S9 PL kinetic in the presence of different ligand concentrations Pag. S7

Fig. S10 PL and PLE spectra of **L-AIS** isolated after first and second reaction step Pag. S8

Fig. S11 XRD data of **L** and **D-AIS** isolated after first and second reaction step Pag. S8

Investigation on the second reaction step: chiroptical activity Pag. S9

Fig. S12 CD and UV/Vis spectra of **L-AIS** QDs solutions Pag. S9

Fig. S13 CD spectra of **L-AIS** in different ligand concentration collected after different time delay Pag. S10

Fig. S14 ^{1}H-NMR spectra of a solution of L-Cys 16.0 mM in D_2O Pag. S11

Fig. S15 NOESY analysis of **L-AIS** QDs in the presence of a ligand concentration of 4.0 mM Pag. S12

Fig. S16 UV/Vis spectra of **L-AIS** QDs solution in the presence of different ligand concentrations Pag. S12

Dosy NMR Investigation and quantification of the free and bonded populations Pag. S13

Table S2 Calculated data on the ligand populations Pag. S13

Fig. S17 Plot of the molar fraction and number of mol of free and bonded ligand Pag. S14

Fig. S18 DOSY analysis of **L-AIS** QDs solution in the presence of different concentration of L-Cys Pag. S15

Fig. S19 CD spectra of **L-AIS** QDs in the presence of L-Cys concentration of 100.0 mM Pag S16

References Pag. S17

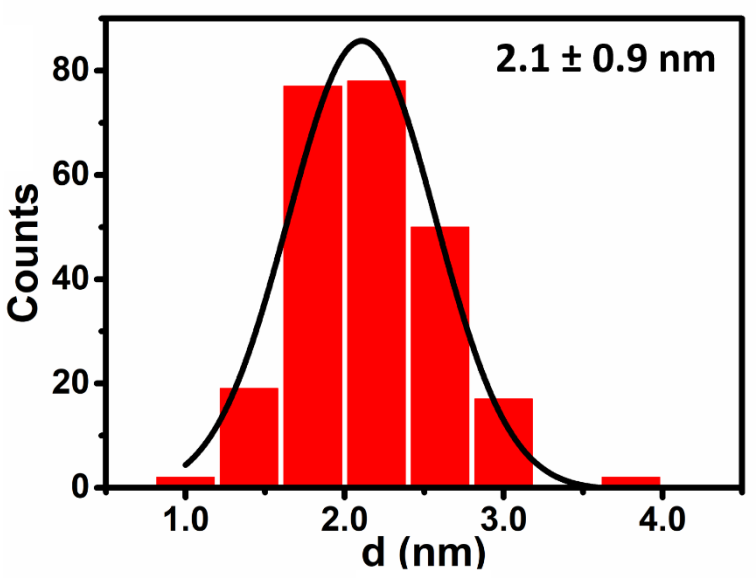

Fig. S1 Particle size distribution based on the measurement on 300 nanocrystals.

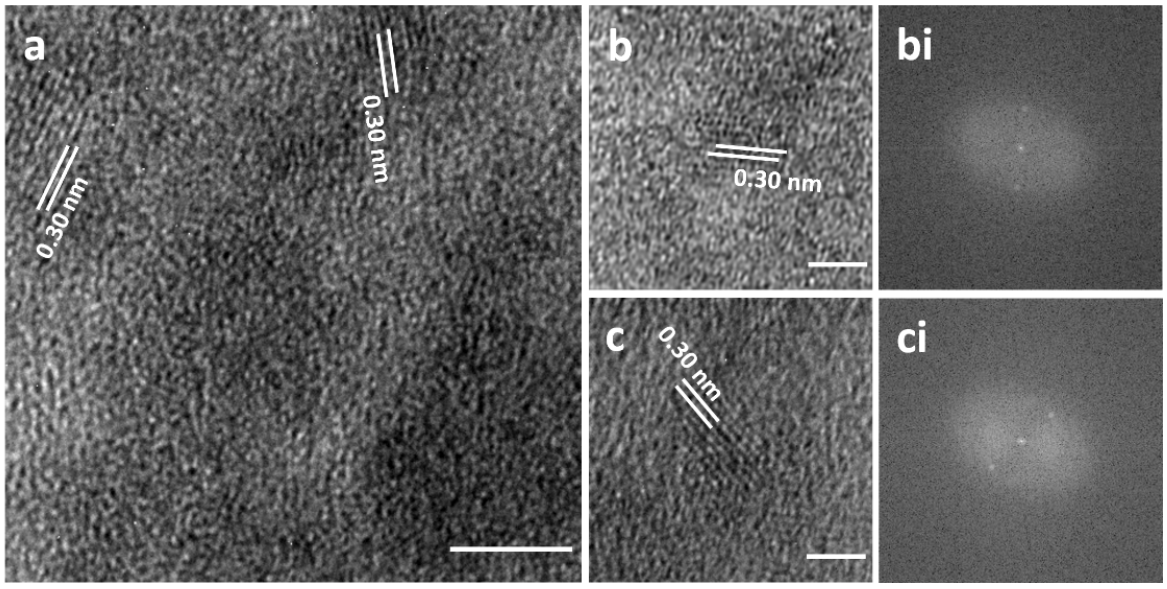

Fig. S2 (a-c): phase contrast TEM images of non-stoichiometric AIS QDs, scale bars: a = 4.0 nm; b and c = 2.0 nm; (bi), (ci): Fourier Transform images of b and c, respectively.

XPS analysis

A large part of the detected carbon is due to contamination from the atmosphere, originating a band at very low BE related to hydrocarbons and usually used for evaluating the surface charging in non-conductive samples. We assumed this signal to be centered around 248.8 eV, even if the use of carbon contamination as standard for BE correction is currently under strong debate:[1] Our actual choose gives however a consistent picture of the physical-chemical state of the sample surface, starting from the BE positions consequently determined.

Deconvolution of the C 1s (**Fig. S3a**) band shows the compresence of three contributes, related to the presence of hydrocarbon contamination and of chiral ligand: the main one is fixed at 284.8 eV and is related to C-C and/or C-H bonds (as reported above), the second one falls at 286.5 eV and is related to C-S and/or C-N bonds, and the last one falls at 288.6 eV and is attributed to C-O bonds.[2] N1s signal (**Fig. S3b**) shows the presence of two contributes centered around 399.9 eV and 401.7 eV, related to the compresence of $-NH_2$ and $-NH_3^+$ respectively,[3] according to the protonation state of the cysteine molecules after the purification. The O1s (**Fig S3c**) signal is the overlap of two contribution: the first, falling at 530.6 eV, is mainly related to the ligand C-O bonds,[2] the second is centered around 533.0 eV and can be related to the presence of hydroxides (possibly In-OH groups) and water contaminant.[4,5] The S2p signal (**Fig. S3d**) can be deconvoluted considering the presence of two contributions: the most intense signal falling at 161.5 eV can be related to sulfide anions S^{2-} and thiolate groups $C\text{-}S^-$, the second signal centered at 164.1 eV can be related to protonated cysteine thiol groups C-SH or to the disulfide dimer cystine CS-SC.[2,3,6]

Silver presence originates the characteristic 3d band (**Fig. S3e**), showing the $3d_{5/2}$ component centered at 367.9 eV (for a spin-orbit splitting, SOS, of 6.1 eV). The $Ag3d_{5/2}$ binding energy is not very sensitive to the change of the chemical environment of silver atoms; however, the detected BE value is closer to literature data for Ag^+ than Ag^0.[7] In3d (**Fig. S3f**) band is the main signal of indium, whose main component $3d_{5/2}$ is centered at 444.8 eV (7.6 eV of SOS). The detected binding energy suggests the presence of In^{3+}, related to indium sulfide and possibly to small amount of oxide. Between the experimental uncertainties, all the reported attributions are consistent with the quantitative analysis for the different elements.

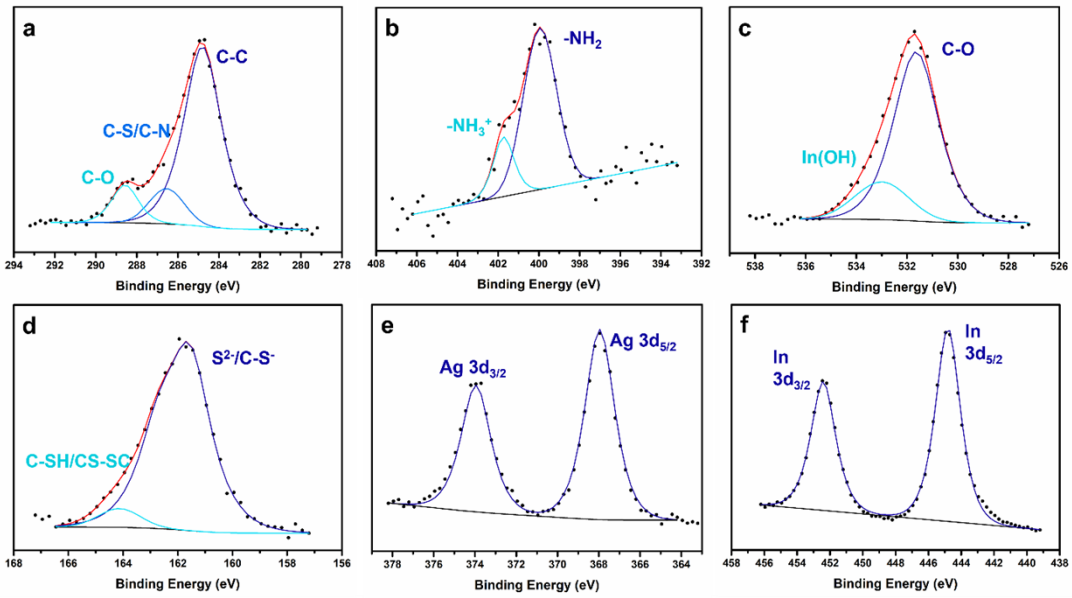

Fig. S3 XPS spectra related to a) C 1s, b) N 1s, c) O 1s, d) S 2p, e) Ag 3d and f) In 3d. The baseline is indicated in black and the sum of different components (if any) employed in the fitting process is reported in red.

Photoluminescence Quantum Yield Determination:

Equation S1[8,9]

$$\Phi_{QDs} = \Phi_{st}\frac{I_{QDs}f_{st}n_{QDs}^2}{I_{st}f_{QDs}n_{st}^2} \quad \text{(S1)}$$

The subscripts *QDs* and *st* refer to the quantum dots or the fluorescence standard respectively. The PLQY is represented by Φ, I represent the integrated intensity corrected by the fluorimeter sensitivity and the source intensity, n represents the diffraction index of the solvent and f the absorption factor

Equation S2[8,9]

$$f_{QDs,st} = 1 - 10\hat{}(-A_{QDs,st}) \quad \text{(S2)}$$

Where f and A represent the absorption factor and the absorbance for quantum dots (*QDs*) and fluorescence standard (*st)*.

Photoluminescence Lifetime Analysis

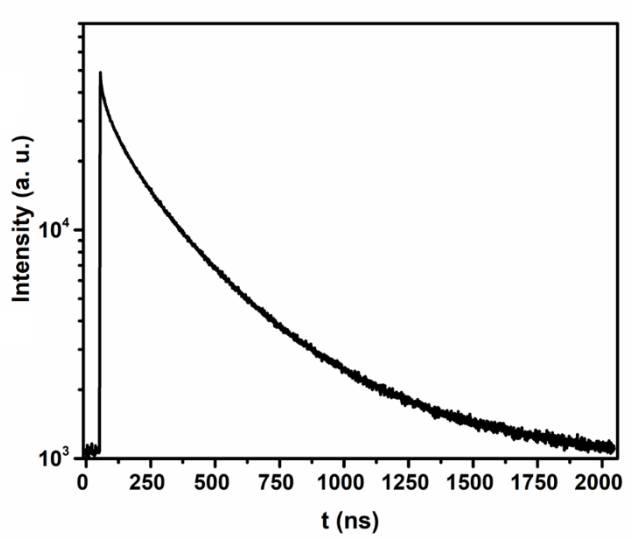

Fig. S4 PL decay curve of **L-AIS** QDs solution

Equation S3

$$I(t) = A_1 e^{-\frac{t}{\tau_1}} + A_2 e^{-\frac{t}{\tau_2}} + A_3 e^{-\frac{t}{\tau_3}}$$

I(t) represents the linear combination of three single-exponential functions, where A_i are the amplitudes and τ_i are the time constants of the separate single-exponential terms.

Table S1 Lifetimes and amplitudes obtained from the fit of the PL decay curve.

τ_1 (ns)	169.6
A1	0.33
τ_2 (ns)	606.3
A2	0.41
τ_3 (ns)	21.0
A3	0.19

Equation S4

$$\tau_{Av} = \frac{\sum A_i \tau_i^2}{\Sigma A_i \tau_i}$$

Where τ_{Av} is the average photoluminescence lifetime calculated by weighting the different components of the fitting functions.

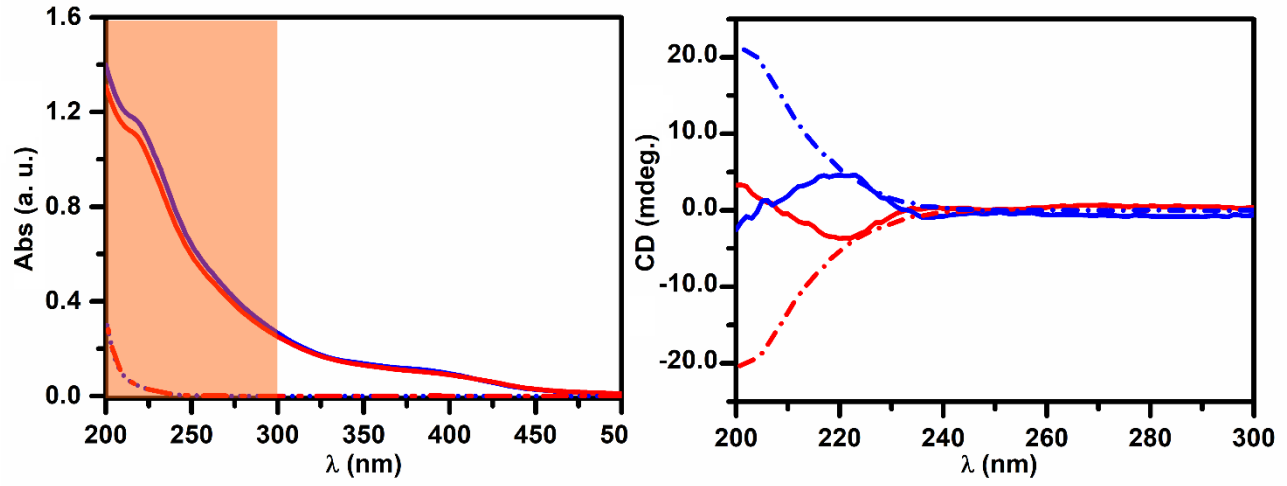

Fig. S5 UV/Vis (left) and CD (right) of **L-AIS** (blue solid line) and **D-AIS** (red solid line) and L-cysteine (blue dashed line) and D-cysteine (red dashed line). The highlighted area (in orange) in the UV/Vis absorption spectrum represents the optical window interested by the CD analysis.

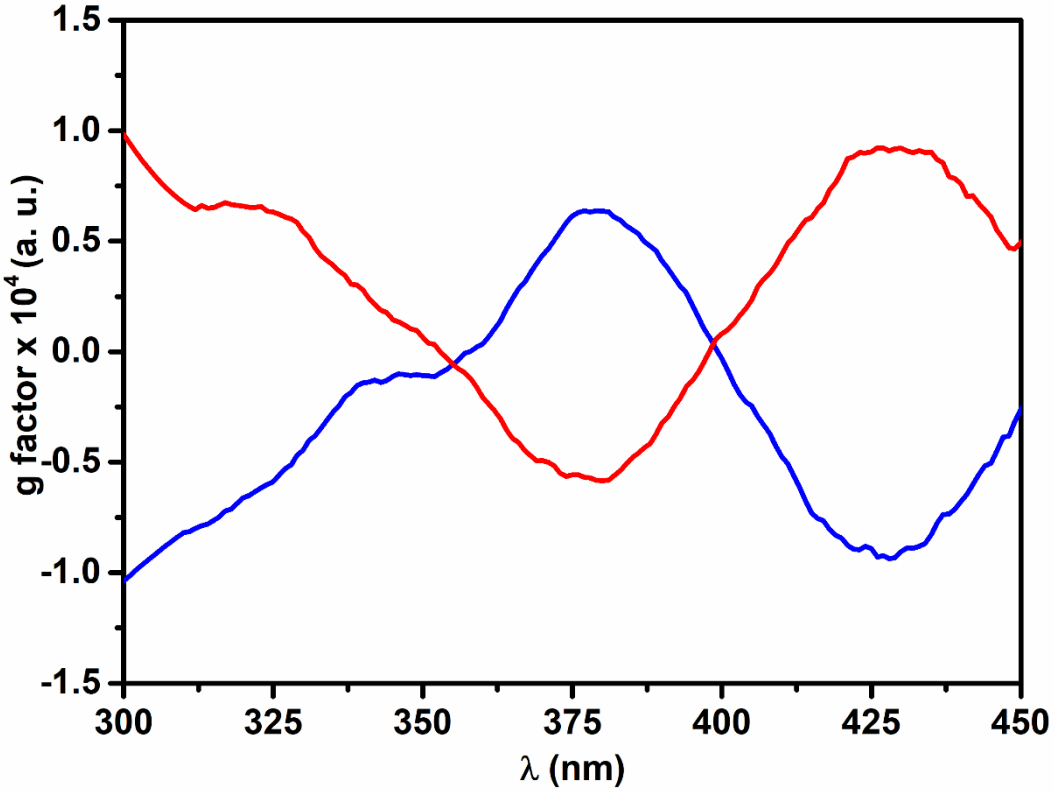

Fig. S6 Anisotropic g-factor of L-AIS (blue line) and D-AIS (red line) QDs stabilized in a 16.0 mM solution of L- or D-cysteine, respectively.

INVESTIGATION ON THE 2nd STEP:

Photoluminescence and structure: the QDs obtained by the 1st step were dispersed in double distillate water at the concentration of 3.0 mg/ml in the presence of a specific amount of chiral ligand. Then, the pH of the solution was adjusted at 7.4with the addition of few microliters of NaOH 0.1 M. As mentioned in the main text, this step is fundamental to enhance the stability and optical properties (photoluminescence and chirality) of the nanocrystals.
As can be appreciated by Fig. S7, which shows the relative emissions of colloidal solutions in different ligand concentrations and Fig. S8 shows the CD spectra of the AIS QDs after dispersion at pH 11.4 without the addition of further ligand.
The PL kinetics analysis shown in Fig. S9 evidences the integrated intensity of the emission band at different time intervals after stabilization of the QD solution in the presence of different L-Cys concentrations (4.0, 8.0 and 16.0 mM). A gradual increase of the photoluminescence is observed for all the ligand concentration up to 300 min. Higher rates are observed for colloids with higher L-Cys concentration; times above 300 min the PL intensities reach a constant value, with a clear dependence on the ligand concentration.
Fig. S11 shows the XRD patterns of the nanocrystals isolated before and after a 24 h of ageing in the presence of a ligand concentration of 48.0 mM, evidencing a clear increase of the nanocrystals crystallinity by the narrowing of the FWHM of all the diffraction reflections.

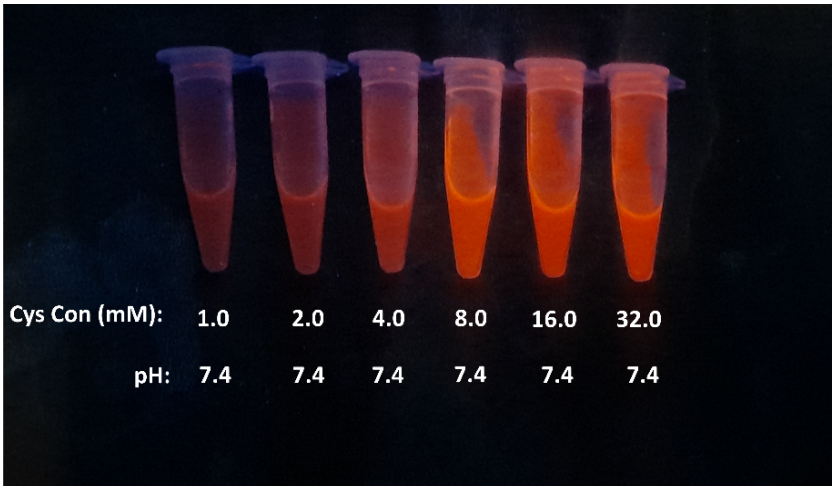

Fig. S7 L-AIS colloidal dispersions with different ligand concentration under UV lamp (λ = 365 nm).

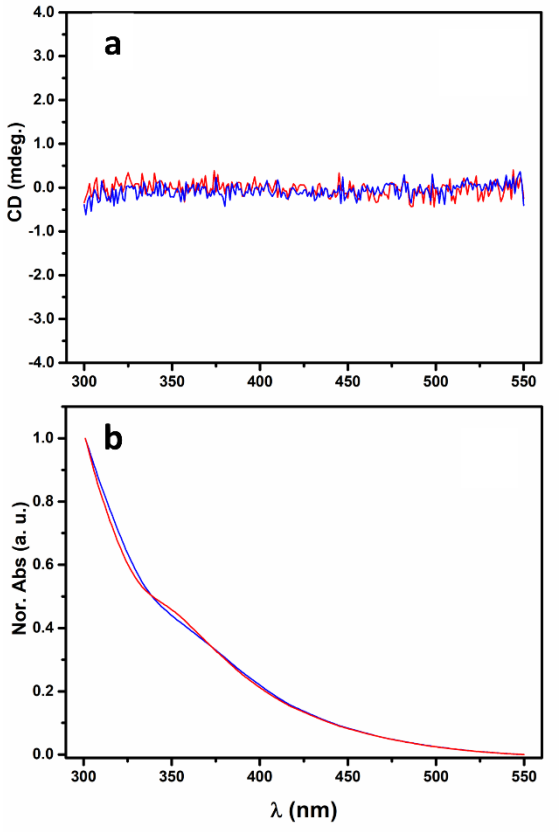

Fig. S8 CD spectra (a) and UV/Vis (b) of the solution of nanocrystals isolated after the 1st step in the presence of L (blue) or D (red) cysteine after dispersion at pH 11.4.

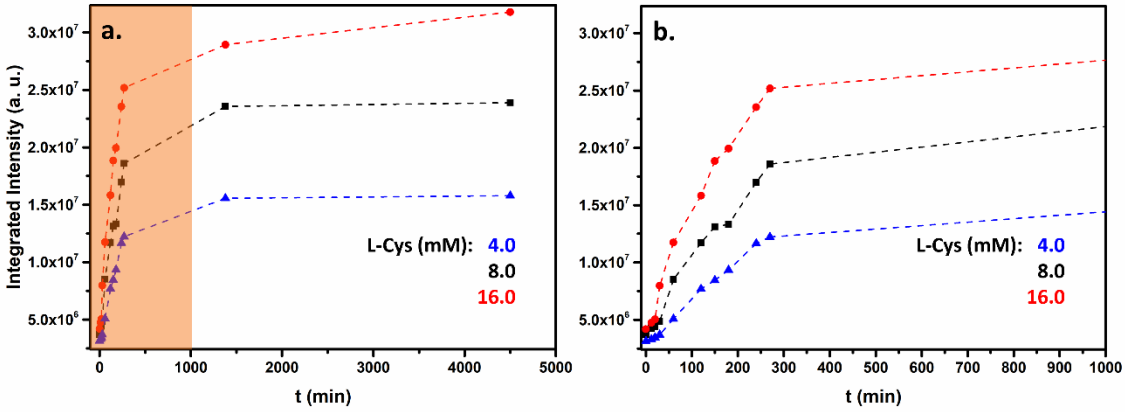

Fig. S9 a) PL integrated intensity vs time of QDs dispersions for different L-Cys concentrations. b) Magnification of the 0-1000 min region (highlighted in orange in Fig. S9a).

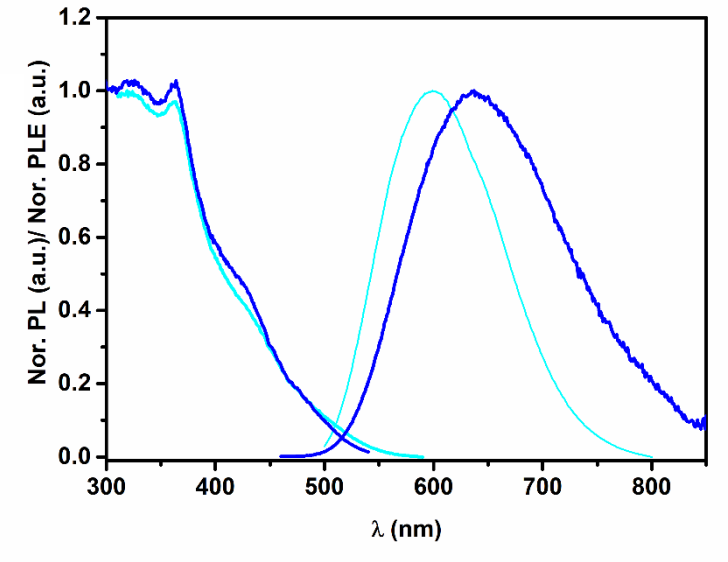

Fig. S10 PL and PLE spectra of the nanocrystals isolated after the 1st (light blue) and 2nd (blue) step respectively.

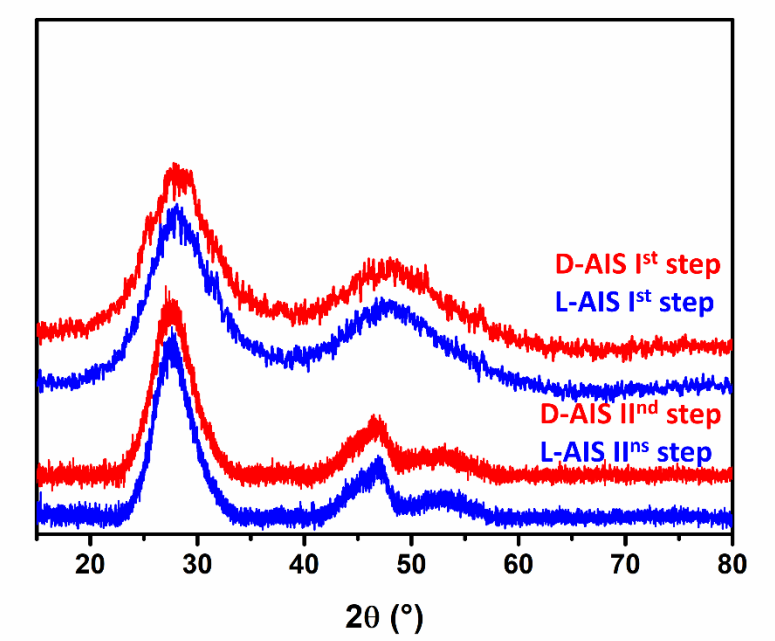

Fig. S11 XRD data of the QDs isolated at the different step of the synthesis, the pattern for the nanocrystals produced in the presence of L or D-Cys are indicated in blue and red respectively.

Chiroptical activity: even if the particles isolated before the ageing step present clear chiroptical properties (Fig. S12 a,b) these are readily lost in few hours after redispersion in absence of a certain chiral ligand concentration (Fig. S8) probably due to the dissociation of the chiral ligand.
Differently, for AIS in 16.0 mM concentration of L-Cys, the CD bands centered at 310 and 335 nm show a gradual decrease and an increase of the bands around 400 nm is observed (Fig. S12 c,d) The process needs more than 32 h up to 48 h to be completed for QD solutions stabilized in a ligand concentration of 16.0 mM.
Further investigations on this process considering different L-Cys concentrations (8.0, 25.0, 50.0 and 100.0 mM) show that the transition is accelerated on increasing the ligand concentration from 8.0 to 100.0 mM (**Fig. S13**), reaching a condition at which the bands at 310 and 335 nm disappear even after 6 h, as can be observed for the sample stabilized at the highest L-Cys concentration.

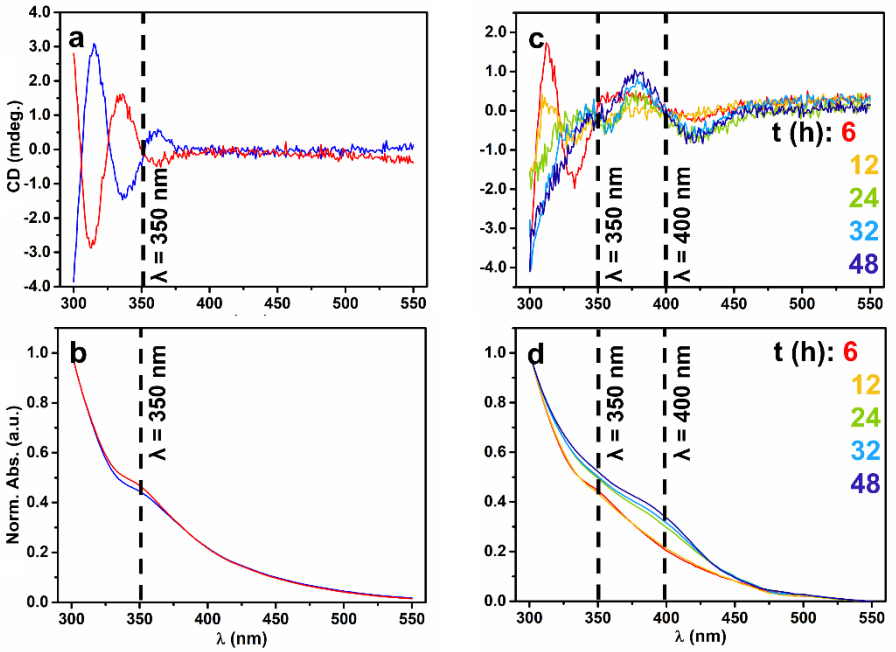

Fig. S12 CD and UV/Vis spectra of fresh colloidal solutions of nanocrystals at the end of the first reaction step, produced in the presence of L (blue) or D (red) Cys. CD (c) and UV/Vis (d) spectra of the nanocrystals collected at different time delays after the particle stabilization in the presence of 16 mM of L-Cys.

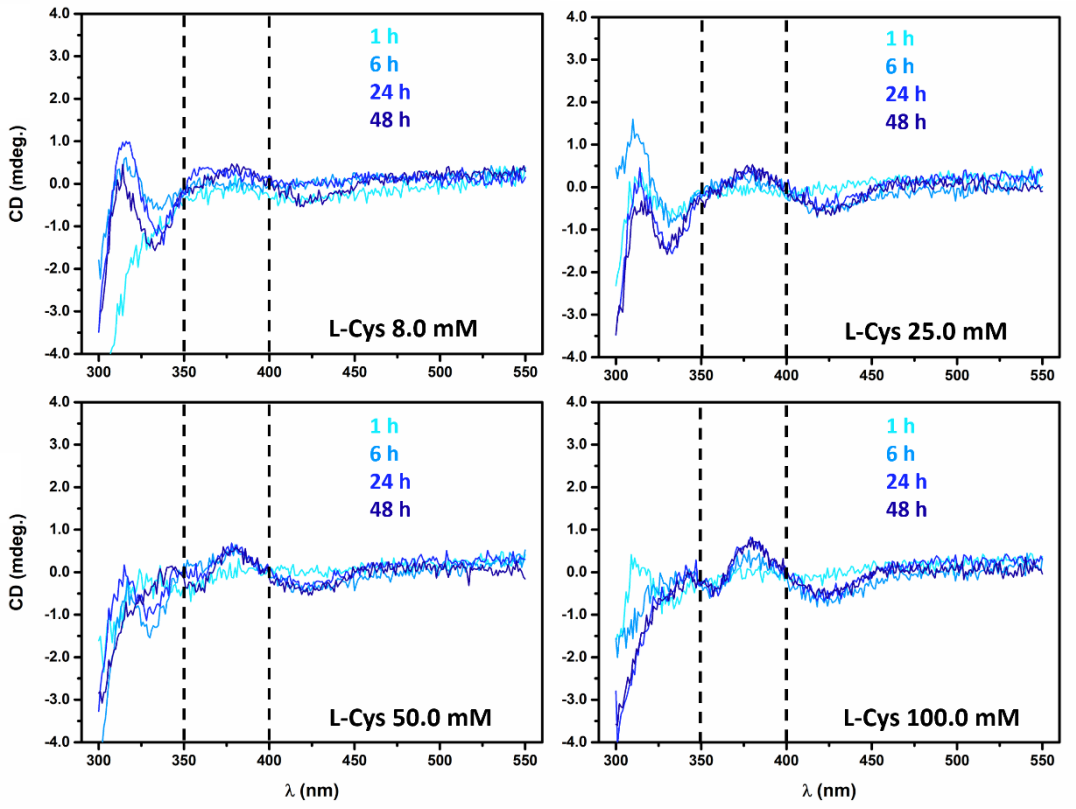

Fig. S13 CD analysis of the aging process for **L-AIS** QDs at different L-Cys concentrations collect at different time delay.

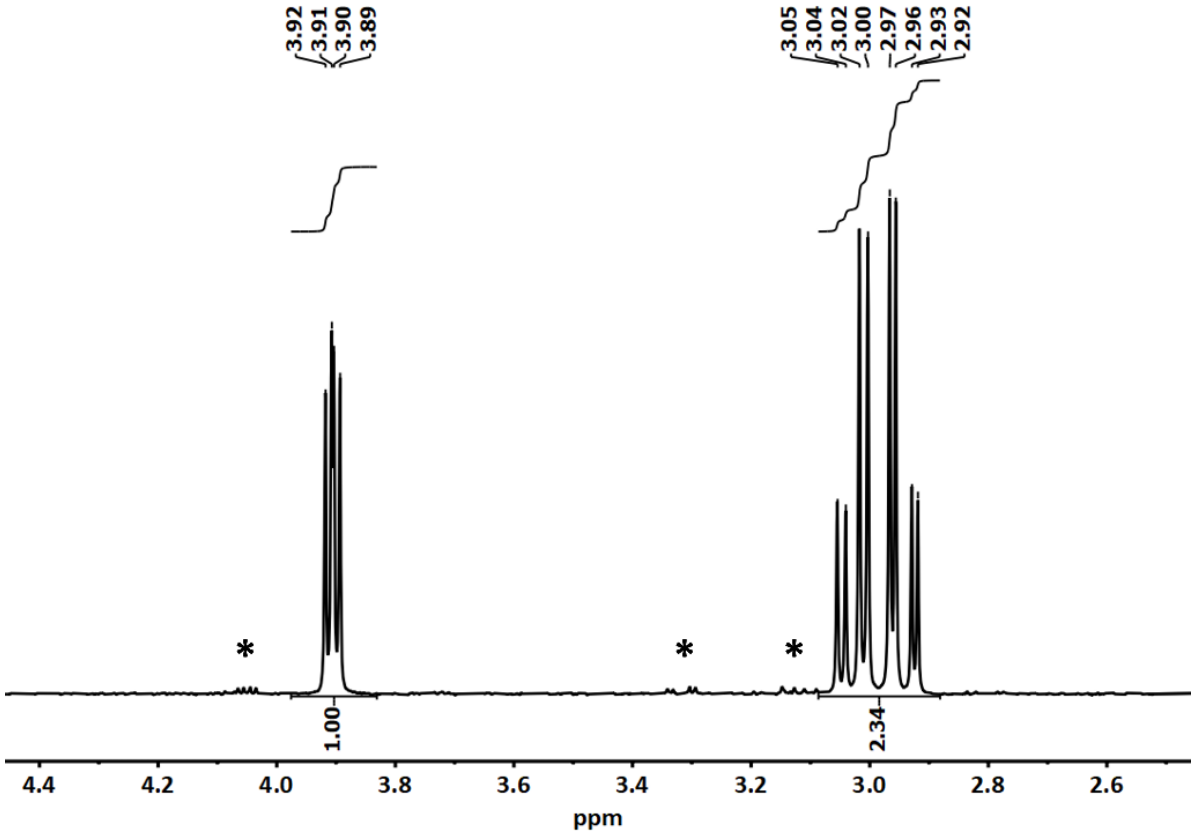

Fig. S14 ^{1}H-NMR spectra of a solution of L-Cys 16.0 mM in D_2O, the signals from L-cystine are marked with an asterisk.

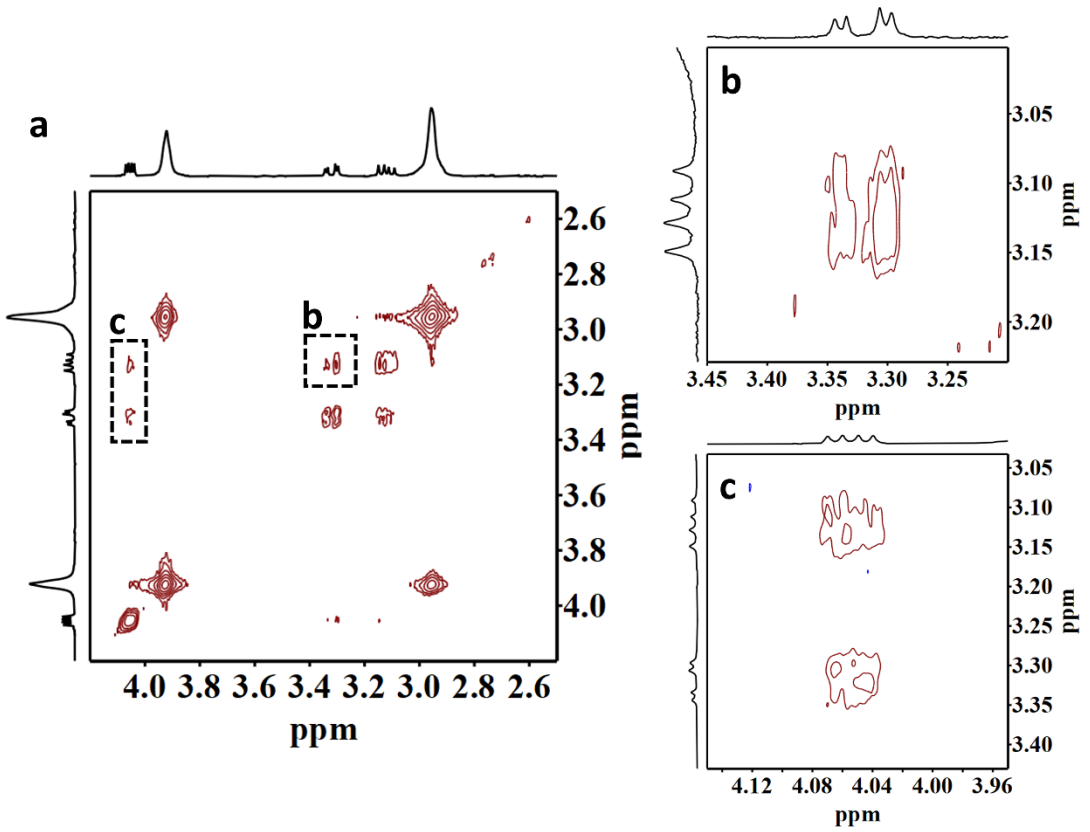

Fig. S15 a) NOESY analysis of a **L-AIS** QDs solution in the presence of 4.0 mM L-Cys. B and c) expanded areas of the L-cystine negative cross peaks.

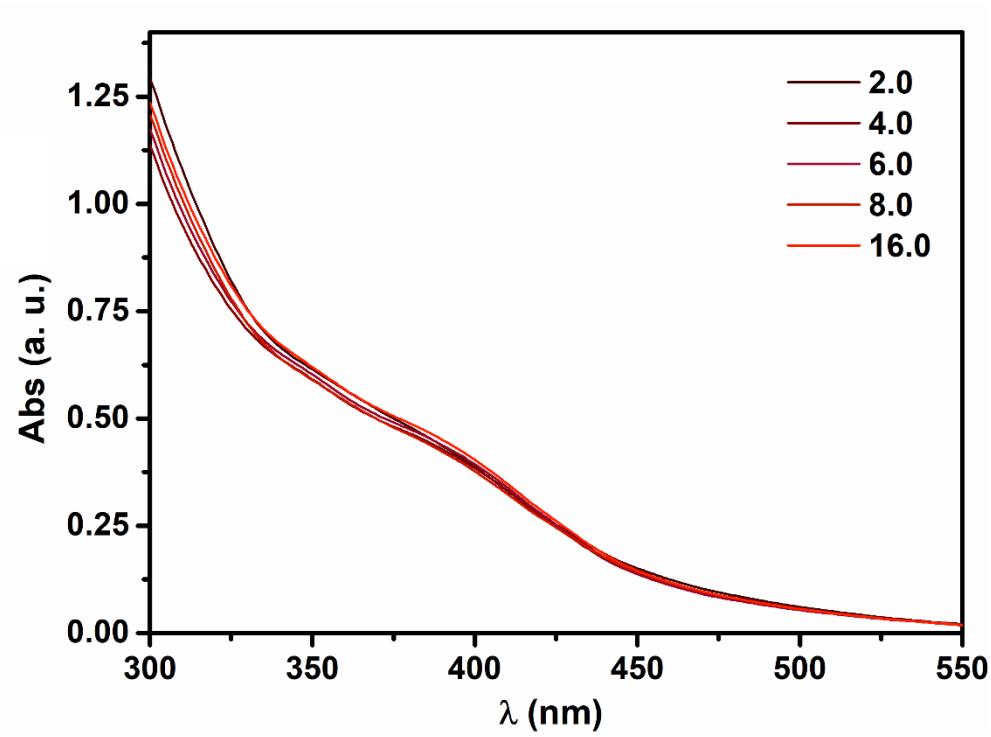

Fig. S16 UV/Vis spectra of the AIS colloidal solution in different ligand concentrations.

DOSY NMR and Quantification of the Free and Bonded Populations

Equation S5[10–12]

$$D_i = x_b D_b + (1 - x_b) D_f$$

Equation S6

$$x_b + x_f = 1$$

Where D_i correspond to the measured diffusion coefficient at the i_{th} ligand concentration, D_b and D_f are the diffusion coefficient for the bonded ($D_b = D_{2.0mM} = 4.36 \times 10^{-10}$ m^2/s) and free ($D_f = 12.0 \times 10^{-10}$ m^2/s) ligand. Finally, x_b and x_f correspond to the molar fraction of the ligand in the bonded and free form respectively.[13]

Table S2 calculated data on the ligand populations

M (mM)	**D_i x10^{-10} m^2/s**	**x_b** -	**x_f** -	**n_{tot} (mol)**	**n_b (mmol)**	**n_f (mmol)**
4.0	6.92	0.66	0.34	2.80E-06	1.86E-03	9.38E-04
6.0	7.41	0.60	0.40	4.20E-06	2.52E-03	1.68E-03
8.0	8.32	0.48	0.52	5.60E-06	2.70E-03	2.90E-03
16.0	9.12	0.38	0.62	1.12E-05	4.22E-03	6.98E-03

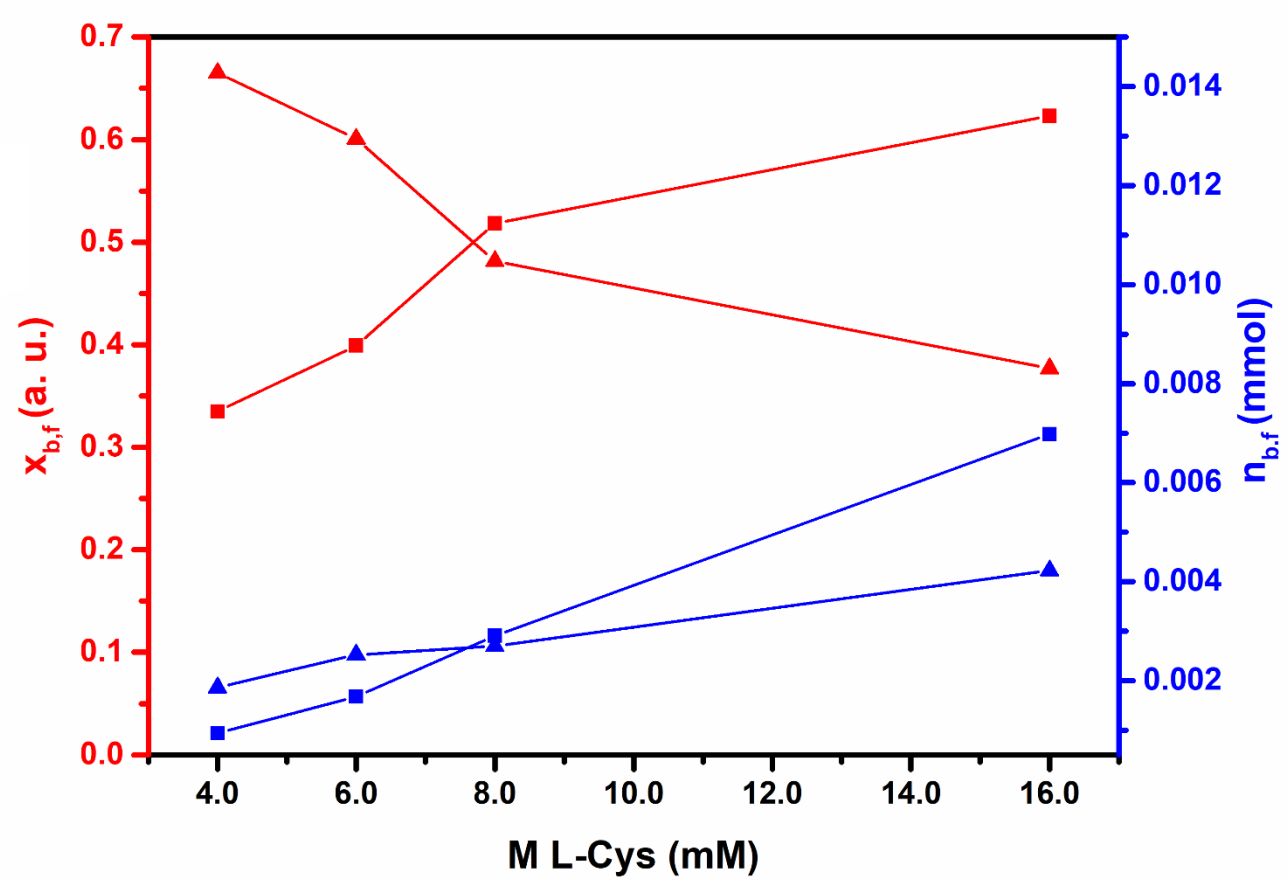

Fig. S17 Calculated molar fractions ($x_{b,f}$) and mole number ($n_{b,f}$) for the bonded (triangle) and free (square) forms of the ligand.

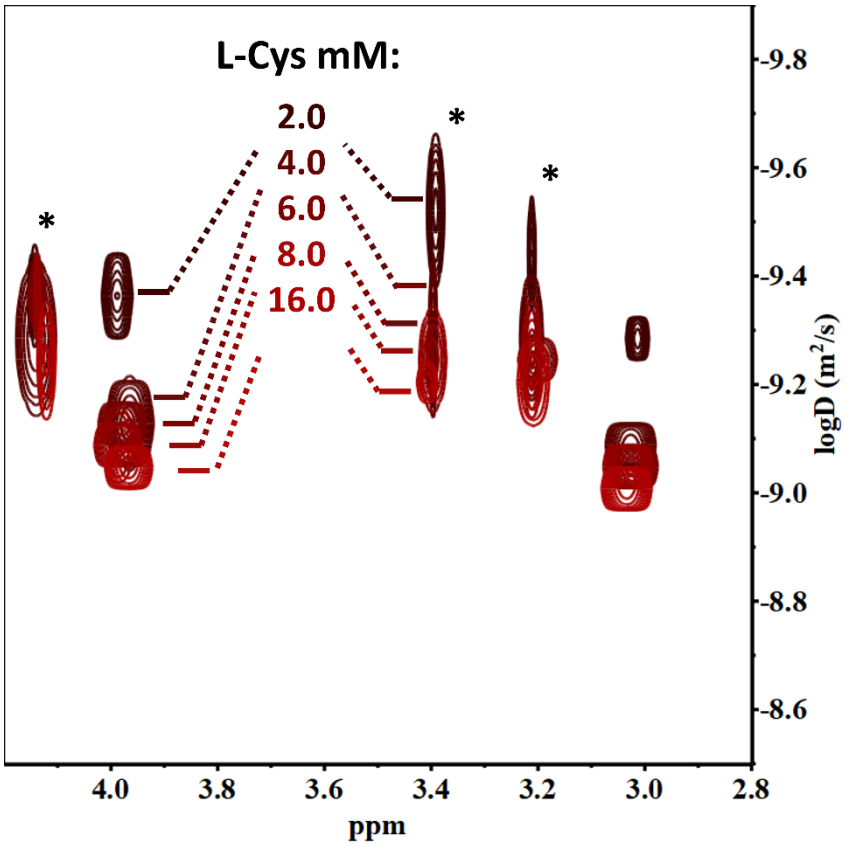

Fig. S18 DOSY analysis of **L-AIS** QDs solution in the presence of different concentration of L-Cys. The signals from L-cystine are marked with an asterisk.

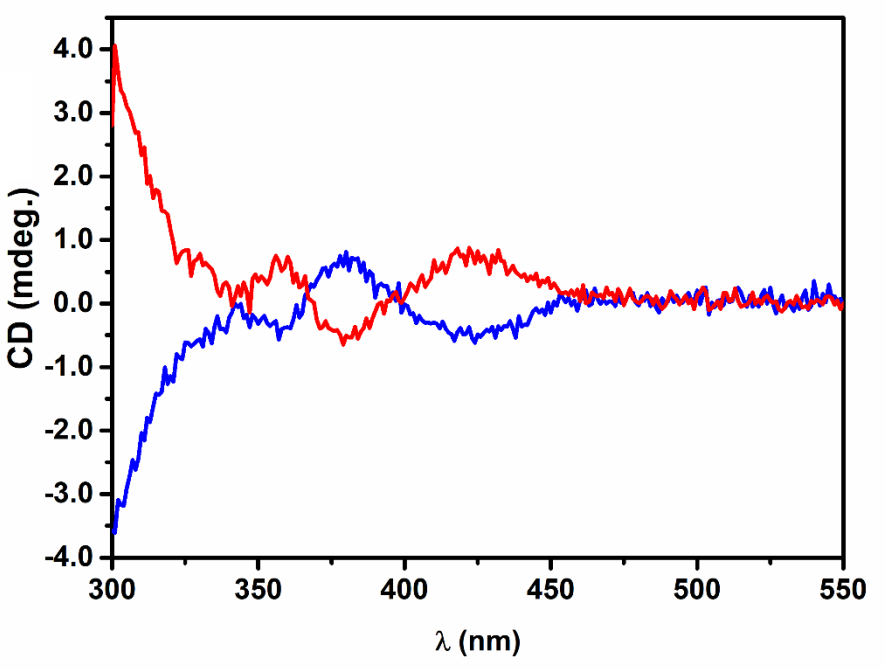

Fig. S19 CD spectra of **L-AIS** (blue) and **D-AIS** (red) in the presence of a ligand concentration of 100.0 mM at pH 7.4

REFERENCES:

1 G. Greczynski and L. Hultman, *Sci. Rep.*, 2021, **11**, 11195.

2 R. C. M. Salles, L. H. Coutinho, A. G. Veiga and M. M. Sant'Anna, *J. Chem. Phys.*, 2018, **148**, 045107.

3 G. Gonella, S. Terreni, D. Cvetko, A. Cossaro, L. Mattera, O. Cavalleri, R. Rolandi, A. Morgante, L. Floreano and M. Canepa, *J. Phys. Chem. B*, 2005, **109**, 18003–18009.

4 C. N. Carvalho, A. M. B. Rego, A. Amaral, P. Brogueira and G. Lavareda, *Surf. Coat. Technol.*, 2000, **124**, 70–75.

5 L. B. Hoch, T. E. Wood, P. G. O'Brien, K. Liao, L. M. Reyes, C. A. Mims and G. A. Ozin, *Adv. Sci.*, 2014, **1**, 1400013.

6 W. Xiang, C. Xie, J. Wang, J. Zhong, X. Liang, H. Yang, L. Luo and Z. Chen, *J. Alloys Compd.*, 2014, **588**, 114–121.

7 NIST X-ray Photoelectron Spectroscopy Database, NIST Standard Reference Database Number 20, National Institute of Standards and Technology, Gaithersburg MD, 20899 (2000), doi:10.18434/T4T88K.

8 U. Resch-Genger and K. Rurack, *Pure Appl. Chem.*, 2013, **85**, 2005–2026.

9 A. M. Brouwer, *Pure Appl. Chem.*, 2011, **83**, 2213–2228.

10 C. S. Johnson, *J. Magn. Reson. A*, 1993, **102**, 214–218.

11 E. J. Cabrita and S. Berger, *Magn. Reson. Chem.*, 2002, **40**, S122–S127.

12 E. J. Cabrita, S. Berger, P. Bräuer and J. Kärger, *J. Magn. Reson.*, 2002, **157**, 124–131.

13 X. Ji, D. Copenhaver, C. Sichmeller and X. Peng, *J. Am. Chem. Soc.*, 2008, **130**, 7012–7021.